Scientific Reports

https://doi.org/10.1038/s41598-026-42482-3

Article in Press

Machine learning–assisted evolutionary optimization of hole quality and surface integrity in abrasive waterjet drilling of polycarbonate

Received: 31 December 2025

Accepted: 26 February 2026

Published online: 11 March 2026

Cite this article as: Chandar J.B., Rathinasuriyan C., Lenin N. *et al.* Machine learning–assisted evolutionary optimization of hole quality and surface integrity in abrasive waterjet drilling of polycarbonate. *Sci Rep* (2026). https://doi.org/10.1038/s41598-026-42482-3

J. Bharani Chandar, C. Rathinasuriyan, N. Lenin, M. Sivakumar, Robert Čep & Sachin Salunkhe

We are providing an unedited version of this manuscript to give early access to its findings. Before final publication, the manuscript will undergo further editing. Please note there may be errors present which affect the content, and all legal disclaimers apply.

If this paper is publishing under a Transparent Peer Review model then Peer Review reports will publish with the final article.

ARTICLE IN PRESS

© The Author(s) 2026. **Open Access** This article is licensed under a Creative Commons Attribution-NonCommercial-NoDerivatives 4.0 International License, which permits any non-commercial use, sharing, distribution and reproduction in any medium or format, as long as you give appropriate credit to the original author(s) and the source, provide a link to the Creative Commons licence, and indicate if you modified the licensed material. You do not have permission under this licence to share adapted material derived from this article or parts of it. The images or other third party material in this article are included in the article's Creative Commons licence, unless indicated otherwise in a credit line to the material. If material is not included in the article's Creative Commons licence and your intended use is not permitted by statutory regulation or exceeds the permitted use, you will need to obtain permission directly from the copyright holder. To view a copy of this licence, visit http://creativecommons.org/licenses/by-nc-nd/4.0/.

ARTICLE IN PRESS

Machine Learning–Assisted Evolutionary Optimization of Hole Quality and Surface Integrity in Abrasive Waterjet Drilling of Polycarbonate

Bharani Chandar J[1], Rathinasuriyan C[1*], Lenin N[2], Sivakumar M[2], Robert Čep[3], Sachin Salunkhe[4]

[1]*Department of Mechanical Engineering, Vel Tech Rangarajan Dr. Sagunthala R&D Institute of Science and Technology, Tamil Nadu-600 062, India*

[2]*Department of Mechanical Engineering, SRM TRP Engineering College, Tamil Nadu-621 105, India*

[3]*Department of Machining, Assembly and Engineering Metrology, Faculty of Mechanical Engineering, VSB-Technical University of Ostrava, 17. Listopadu 2172/15, 708 00 Ostrava, Czech Republic;*

[4a]*Department of Biosciences, Saveetha School of Engineering, Saveetha Institute of Medical and Technical Sciences, Chennai, India*

[4b]*Department of Mechanical Engineering, Gazi University Faculty of Engineering, Maltepe, Ankara, Turkey*

*Corresponding author: rathinasuriyanphd@gmail.com

ARTICLE IN PRESS

Abstract

Abrasive Waterjet Machining (AWJM) is a reliable non-traditional technology for machining polymer-based engineered materials with low thermal degradation, dimensional inaccuracy, and surface damage. This study examines polycarbonate hole drilling performance using 125 full-factorial experimental trials using process parameters water pressure, standoff distance, and traverse rate. With a coordinate measuring machine and stylus-based profilometer, kerf angle, entry and exit circularity, and surface roughness were measured in a detailed metrological research. Four ML models were created to develop accurate predicting capabilities, with the Random Forest (RF) model performing best in all responses. RF predicted processes accurately with high coefficient-of-determination R^2 values (0.92, 0.82, 0.82, and 0.92) and low error coefficients (RMSE 0.196, 0.045, 0.042, and 0.452). The best drilling settings were found using evolutionary algorithms like Biogeography-Based Optimization (BBO),

ARTICLE IN PRESS

Particle Swarm Optimization (PSO), Salp Swarm Optimization (SSO), and Tug-of-War Optimization (TWO). Deng's similarity metric ranked SSO as the best optimizer based on many responses. The SSO produced the optimal settings (W_p = 250 MPa, S_d = 1.5, and T_r = 300 mm/min) for reduced kerf deviation, circularity and surface roughness. Under optimal circumstances, anticipated responses matched experimental results, proving the integrated ML-optimization framework's strength.

Keywords: *abrasive waterjet drilling; process parameter; machine learning; optimization*

Introduction

The polycarbonate has found extensive usage in optical, biomedical, aerospace and defense applications due to its great impact strength, dimensional stability and optical transparency. Its machinability has been investigated in various conventional and non-conventional processes with each offering specific difficulties and optimization demands. In abrasive jet micromachining, Getu et al. demonstrated that erosion rate in PMMA, acrylic, and PC is highly sensitive to traverse direction at oblique angles, with forward scanning enhancing material removal [2]. They developed an analytical model that accurately predicted micro-channel and micro-hole profiles. A broader review by Madhu et al. identified Water Pressure (W_p), Standoff Distance (S_d), Traverse Rate (T_r), particle size, and impact angle as the dominant parameters influencing Kerf Angle (K_a) and Surface Roughness (S_r) in composite laminates, reinforcing the importance of parameter control for dimensional accuracy [3]. In mechanical micro-milling, Jahan et al. showed that ductile mode cutting of PC glass can be achieved with optimal combinations of depth of cut and feed rate, reducing cutting forces and improving S_r; finite element modeling effectively predicted these forces for process optimization [4]. Adeniji et al. further reported that burr formation and S_r are governed more by cutting-edge radius, feed rate, and tool edge condition than by depth of cut [5]. Tool wear investigations by Jahan et al. revealed that TiAlN-coated tools significantly reduce adhesion wear compared to uncoated carbide tools, although delamination wear may arise under higher loads; medium cutting

ARTICLE IN PRESS

parameters produced the best compromise between tool life and surface quality. Hybrid and assisted machining approaches have been applied to enhance process performance [6]. Singh et al. optimized chemical-assisted ultrasonic machining of bullet-proof PC glass using Taguchi design, grey relational analysis and response surface methodology, finding that 30% slurry concentration, appropriate grit size, and Nimonic-80A tooling maximized Material Removal Rate (MRR) while minimizing tool wear rate and S_r [7]. In micro-electric discharge machining, Vishwakarma et al. demonstrated that graphene nanoplatelet reinforcement improves conductivity and machinability of PC composites, and that rotating electrodes enhance flushing efficiency, resulting in higher MRR and improved Sr [8]. Laser-based machining of PC has also been studied for micro-feature fabrication. Moradi et al. optimized continuous CO_2 laser micro-drilling, showing that properly selected laser power and cutting speed minimized heat affected zone and taper, with theoretical predictions matching experiments [9]. Similarly, Moradi et al. concluded that reducing focal plane position and laser power, combined with higher cutting speeds, improved K_a quality in low-power CO_2 laser cutting of injection molded PC [10]. In high-precision optical manufacturing, Mishra et al. achieved nanometric S_r (Ra=18.1 nm) and sub-micron form accuracies (Pv=0.116 µm) in ultra-precision diamond turning of PC optics through optimal parameter selection, temperature control, and vacuum clamping. Multi-objective optimization via GRA provided an effective balance between surface finish and profile accuracy [11].

Recent studies on PC processing clearly demonstrate a growing reliance on systematic optimization techniques to enhance surface integrity, mechanical performance, and functional properties. Abdulwahab et al. optimized CO_2 laser micro-drilling of PC using central composite design and response surface methodology, identifying laser power, exposure time, and focal plane position as dominant parameters, with optimized conditions minimizing heat-affected zone and improving hole geometry [12]. Singh et al. applied Taguchi L27 design coupled with grey relational

ARTICLE IN PRESS

analysis to chemical-assisted ultrasonic machining of PC bullet-proof glass, optimizing abrasive size, slurry concentration, power rating, and HF acid content to achieve over 100% improvement in MRR with controlled tool wear and S_r [13]. In additive manufacturing contexts, Meena et al. optimized the S_r of FDM-printed PC spur gears using Taguchi-based abrasive flow finishing, showing that controlled post-processing parameters can drastically reduce S_r [14]. Likewise, Faroze et al. combined dimensional analysis with machine learning to predict and optimize the mechanical properties of FFF-printed polycarbonate components, and supported the fact that data-driven models are superior to purely analytical modeling of complex, nonlinear process-property relationships [15]. Along with structural elements, the optimization strategies have also been applied to functional PC systems. Zahmatkesh et al. used artificial neural networks with multi-objective evolutionary optimization (NSGA-II) in the context of customizing the thermophysical behavior of polycarbonate ultrafiltration membranes [16], and Xiao et al. showed machine-learning-aided material design of fire-safe polycarbonate by effectively sampling large compositional design space. Altogether these studies point to the obvious shift in the traditional single-factor experimentation to combined DOE-ML-evolutionary optimization models that can accommodate several goals and conflicting performance demands [17].

ARTICLE IN PRESS

While optimization methods have been extensively utilized in polycarbonate processing, previous research has predominantly concentrated on additive manufacturing, membrane systems, and material composition. AWJM of polycarbonate received comparatively little focus within integrated machine learning-assisted multi-objective optimization frameworks. Although machine learning–evolutionary optimization techniques have been investigated in the AWJM of metals and composites, their implementation in precision polymer drilling, with simultaneous assessment of various geometric integrity requirements, is still underdeveloped.

ARTICLE IN PRESS

Most current AWJM research on polymers depends on regression-based or single-response optimization models, which may inadequately represent the nonlinear interactions between the jet and polymer that influence dimensional accuracy and surface integrity. This study introduces a comprehensive experimental-computational framework that integrates full-factorial experimentation, comparative machine learning modeling, multi-algorithm evolutionary optimization, and experimental validation to simultaneously predict and optimize Kerf Angle (K_a), Hole Entry Circularity (C_{en}), Hole Exit circularity (C_{ex}), and Surface Roughness (S_r) in polycarbonate drilling.

Material and methods

The current research incorporates a systematic experimental-computational approach and explores the nature of AWJM in the process of drilling holes on polycarbonate sheets. The general workflow of the research incorporates controlled experimentation, precision metrology, prediction with the use of machine learning, and multi-objective evolutionary optimization. This combination can be used to reach a quantitative comprehension of the machining mechanism as well as perform a systematic discovery of the process conditions that reduce quality degradation during polymer drilling. Figure 1 presents the systematic experimental-computational framework.

Polycarbonate was chosen as the working material because it finds a broad spectrum of uses in industries as lightweight structural parts, protective covers and optical housings where the dimensions and the integrity of the surface are very vital [18-20]. A polycarbonate sheet measuring 100 × 100 × 6 mm was used in all the trials to provide uniformity. The specimen was washed with isopropyl alcohol to remove machining residue and surface contaminants which could affect jet interaction. The 6-mm thickness selection follows typical commercial uses and enables consistent assessment of top and bottom geometry during AWJM drilling.

ARTICLE IN PRESS

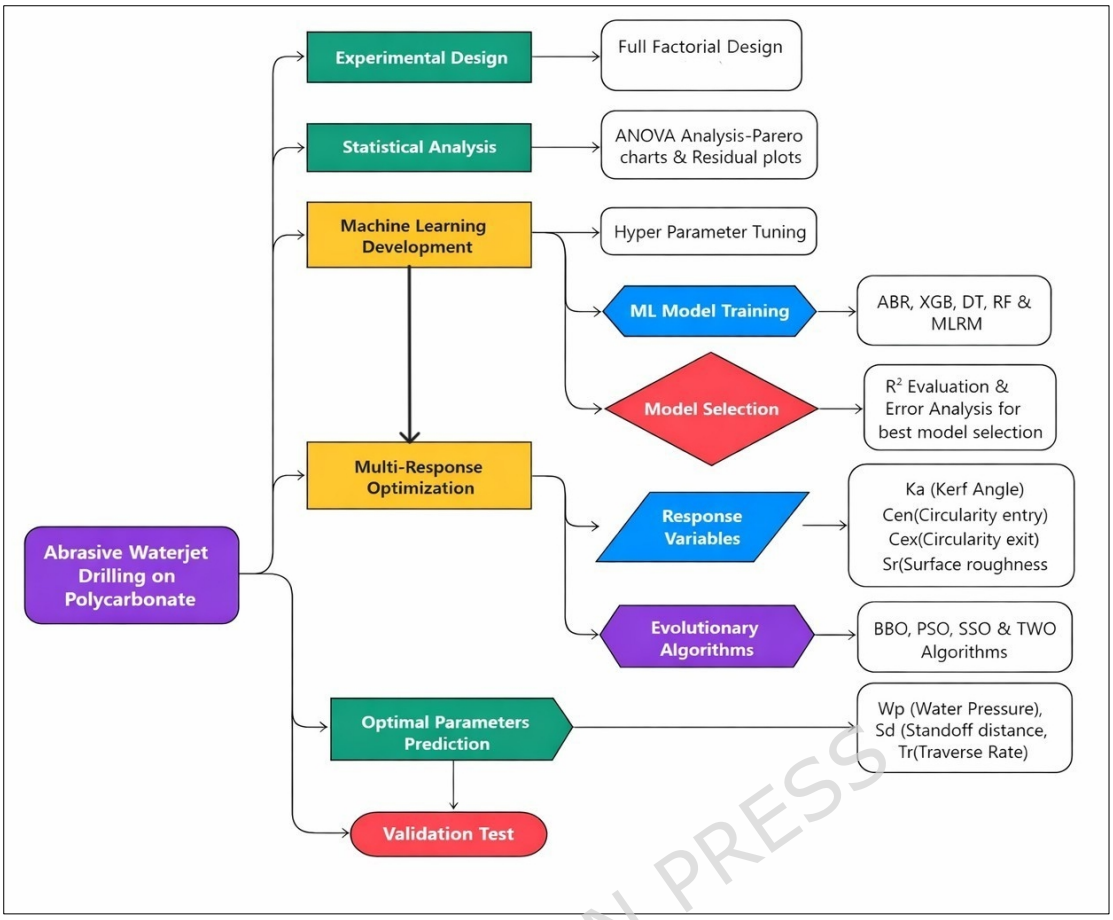

`Figure 1 Experimental-computational framework

The parameters of drilling Polycarbonate were selected using the deformation properties of the material used and the underlying erosion mechanisms due to the jet. One of the dominant factors was chosen to be the water pressure (250MPa-350MPa) due to the fact that it directly influences the kinetic energy of the jet and its impact force which directly affect the efficacy of material removal in polymeric substrates. Standoff distance (1.5 mm-2.5 mm) was varied in the control of jet stability and the attenuation of the energy before interacting with the surface, which had a large impact on the kerf formation and surface quality as the jet dispersion grew. The rate of the traverse (300 mm/min-500 mm/min) was adjusted to manage the time of interaction of the jet and the workpiece so that an optimal balance was established between machining efficiency and surface finish. In order to eliminate the influence of hydraulic parameters, the mass flow rate of abrasive (300 g/min) was constant and this ensured the

ARTICLE IN PRESS

abrasive action was similar and further reduced the variability of the experiment [21-23].

To find out the effect of three important process parameters, a full factorial design of experiment was adopted, W_p, S_d, and T_r. Each of the parameters was assessed on five levels, which created 125 combinations of experiments. This design is adequate to capture the effects of interaction and maintain statistical efficiency. The selection of a 5^3 full factorial design was motivated by the objective of constructing data-driven predictive models rather than fitting predefined polynomial response surfaces. Although RSM and CCD offer experimental efficiency with fewer runs, they are primarily optimized for estimating second-order regression models under assumed quadratic behavior. In contrast, nonparametric machine learning algorithms benefit from dense and uniformly distributed sampling across the design space, which enhances their ability to capture higher-order nonlinear interactions and localized response regimes. The full factorial structure ensures balanced representation of all parameter combinations, reduces extrapolation risk during prediction, and improves model stability when integrated within evolutionary optimization loops. Therefore, the 125-run design was selected to support robust learning of complex jet–polymer interaction behavior rather than to minimize experimental count.

ARTICLE IN PRESS

Pilot tests were used to determine the choice of parameters to use, including those that generate consistent jet shapes and allow quantitative variation of the kerf geometry without leading to thermal distortion and excessive tearing of the polymer substrate. Table 1 presented the parameters of the AWJM used and the levels of the criterion of this study. The detailed full factorial design and its associated outcomes are provided in Supplementary Table S1.

Table 1 AWJM process variables levels and ranges

Parameter	Symbol	Levels	Range
Water Pressure (MPa)	W_p	5 levels	250-350
Standoff Distance (mm)	S_d	5 levels	1.5-2.5
Traverse Rate (mm/min)	T_r	5 levels	300-500

ARTICLE IN PRESS

The drilling experiments were performed on a CNC-controlled AWJM (model: G3020) as illustrated in Figure 2 and set up in such a way as to preserve a constant jet quality over the course of the experimental campaign. The system employed a high pressure intensifier pump (60HP), carbide orifice with a garnet (80 mesh) abrasive feed system as is seen in the state-of-art machining centres. To reduce the deformation caused by vibration workpieces were firmly clamped on a sacrificial backing plate, to ensure that the jet remained stable as the breakthrough took place.



Figure 2 AWJM experimental setup

Each of the drilled holes was measured according to four main response characteristics namely; K_a, C_{en}, C_{ex}, and S_r. The Coordinate Measuring Machine (CMM) with a 0.5 mm ruby stylus was used to carry out the geometric measurements, with traceable ring gauges used to calibrate it. The circularity of each hole was determined by obtaining several boundary points in the hole entry and exit profiles, and then circle-fitting by least-squares. The method provides strong and reproducible estimation of non-circular geometry deviation. The level of surface roughness was measured on the inside of the hole wall by a contact-type stylus gauge using a Gaussian filter (ISO 4287-1997) and normal evaluation length (1 mm). The measurements were again taken around the circumference and an average was taken to be analyzed later. Figure 3 (a and b) respectively show the

ARTICLE IN PRESS

response measurement procedure of circularity and surface roughness respectively. The difference between the entry and exit diameters and the sheet thickness was used to compute the kerf angle, an indicator of jet divergence within the material. The formula to be used to compute the K_a is presented in Equation 1.

$$K_a = \tan^{-1}\left(\frac{D_{ex} - D_{en}}{2T}\right) \quad (1)$$

Where, T-Thickness of the polycarbonate sheet

D_{ex} - Hole exit diameter

D_{en} - Hole entry diameter

In the course of the research, a number of steps were undertaken to guarantee the reliability of the data and its reproducibility. Experiments were done in the randomized order and instruments were recalibrated periodically. Repetition test and standard error-propagation were used to estimate measurement uncertainty.

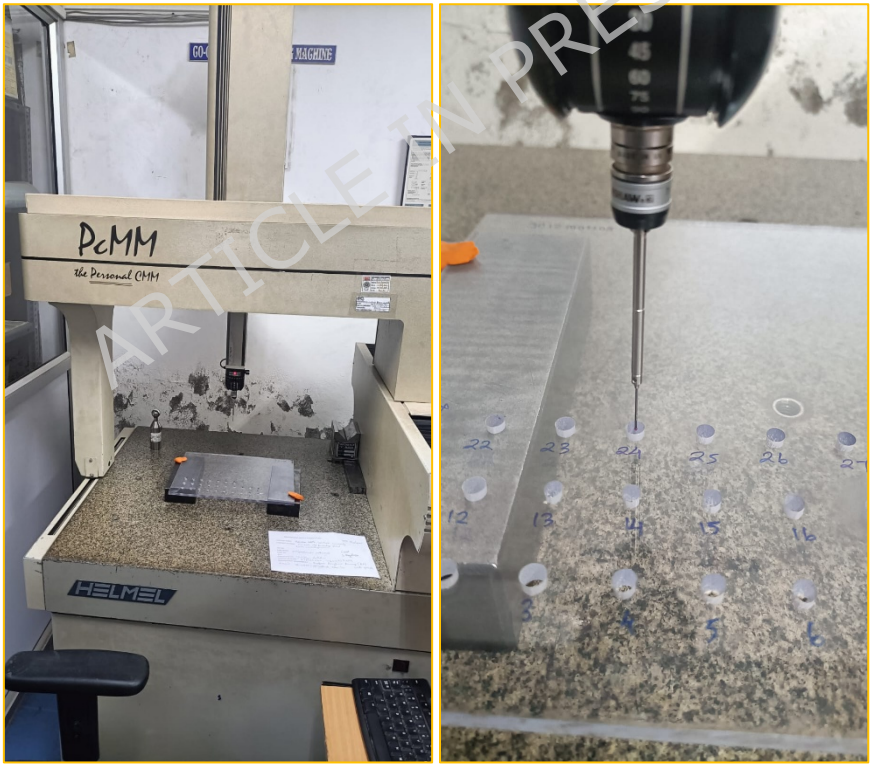

a. Assessment of hole diameter and circularity using CMM

ARTICLE IN PRESS



b. Assessment of surface roughness using contact type stylus instrument

Figure 3 Measurement of geometric and surface integrity characteristics of AWJM-drilled holes

ARTICLE IN PRESS

Integrated Machine learning and algorithmic approach

In order to estimate the correlation between process parameters and machining responses, various machine learning algorithms were designed such as Decision Tree (DT), Random Forest (RF), AdaBoost Regressor (ABR), Extreme Gradient Boosting (XGB), and Multi Linear Regression Model (MLRM). Such models have been selected because they are able to model nonlinear interactions and perform very well on structured experimental data.

Tree-based and ensemble methods such as RF and XGB are particularly effective in handling complex feature interactions, reducing overfitting through aggregation and regularization mechanisms, and providing stable generalization performance without requiring extensive data preprocessing. The chosen algorithms provide practical advantages over alternative models like Artificial Neural Networks (ANN), Support Vector

ARTICLE IN PRESS

Regression (SVR), and Gaussian Process Regression (GPR) for the current investigation. Artificial Neural Network (ANN) models generally necessitate extensive datasets for consistent convergence and exhibit sensitivity to network architecture and weight initialization. The efficiency of SVR is heavily influenced by kernel selection and hyperparameter optimization, potentially escalating computing complexity in multi-response modeling. Gaussian Process Regression, while effective for uncertainty quantification, becomes computationally demanding during iterative evaluations in evolutionary optimization processes. Conversely, ensemble tree-based approaches offer computational efficiency, scalability, less susceptibility to hyperparameter initialization, and consistent performance for nonlinear regression problems using structured experimental data. As a result, these models were deemed better suited for integration with multi-objective evolutionary optimization in the AWJM framework.

The entire dataset was split into training (80 percent) and testing (20 percent) parts. All algorithms were written in custom Python instead of an existing library, which enabled complete control over the learning process and report clear models behaviour. The appropriateness of each of the models was evaluated based on the measures of coefficient of determination, mean absolute error, and root-mean-square error, and the predictive accuracy is the same regardless of the responses.

The fourth stage of the study was minimization, which used four Evolutionary Algorithms (EA) BBO, PSO, SSO and TWO to identify process conditions that optimize the reduction of K_a, C_{en}, C_{ex}, and S_r at the same time. These algorithms were chosen due to their effectiveness in the multi-modal optimization problems that are complex and yet complimentary exploration strategies. Both algorithms worked with the prediction models based on machine-learned models instead of actual experimental data, allowing the rapid and computationally efficient estimation of the optimal combinations of parameters. Table 2 and Table 3 further elaborate on the

ARTICLE IN PRESS

ML and EA that have been selected because of their excellent capability and final setting.

Table 2 ML and EA selection criteria

ML/EA	Strength	Reference
ABR	Enhances predictive robustness by iteratively assigning greater importance to samples with higher prediction errors	24-26
XGB	Achieves superior accuracy through regularized gradient-based learning and efficient modeling of non-linear interactions	
DT	Provides a simple and interpretable framework for capturing input–output relationships with low computational effort	
RF	Improves generalization performance by aggregating multiple decision trees, thereby minimizing overfitting and variance	
BBO	Explores near-global optima using migration-inspired information exchange among candidate solutions	27-30
PSO	Demonstrates rapid convergence by balancing global and local search through collective particle learning	
SSO	Maintains search diversity and avoids premature convergence through salp-based interaction mechanisms among agents	
TWO	Effectively balances exploration and exploitation using force-driven competitive interactions to guide solution evolution	

ARTICLE IN PRESS

Table 3 Final parameter setting of selected algorithms

BBO	Value	PSO	Value	SSO	Value	TWO	Value
Population size (NP)	25	Swarm size (N)	30	Population size (N)	25	Number of teams (N)	30
Immigration rate (I)	1.0	Cognitive coefficient (c_1)	1.8	Salp strength factor (α)	1.5	Force coefficient (α)	0.6
Emigration rate (E)	1.0	Social coefficient (c_2)	1.8	Randomness factor (β)	0.3	Mass updating factor (β)	0.2
Mutation probability (Pm)	0.01	Inertia weight (w)	0.9 → 0.4	Velocity damping factor	0.85	Friction coefficient (μ)	0.05

Results and discussion

ARTICLE IN PRESS

Statistical inferences

In this section, Analysis of Variance (ANOVA) is used to analyze the experimental data to determine the statistically significant process parameters that affect the effectiveness of abrasive water jet machining in terms of kerf angle, circularity, and surface roughness. The ANOVA findings serve as a measure of the relative contribution of main effects, intersection terms and quadratic items obtained by the responsiveness models and also measure the suitability of the models through the estimation of errors. The discussion gives a clear idea of the roles of W_p, S_d, and T_r to the observed responses by correlating statistical significance to physical machining behaviour, which provides a reliable foundation to interpretation and optimization of the process. Minitab software was used to perform ANOVA and the results are presented in Supplementary Tables S2-S5.

Figure 4 indicates that specific governing mechanisms apply to each AWJM response despite the fact that the adequacy of the developed models is confirmed by the percentage contribution analysis. Water pressure dominates the variation in the Kerf angle with the quadratic and linear terms of the pressure fluctuations making an average of 34.7 and 22.7%, respectively, with a total of more than 57% showing a great dependence of the kerf formation on the jet energy and nonlinear amplification, the W_p X T_r interaction (6.4%) and T_r^2 (4.8%) are secondary with the error of the experiment being minimal (6.3%). The pattern of contribution of entry circularity shows the quadratic effect of traverse rate (15.2%), the linear effect of traverse rate (14.4%), and the S_dxT_r interaction (13.2%) are dominant, and terms involving water-pressure influence also play significant roles with moderate and the error is limited to 6.3%.

ARTICLE IN PRESS

ARTICLE IN PRESS

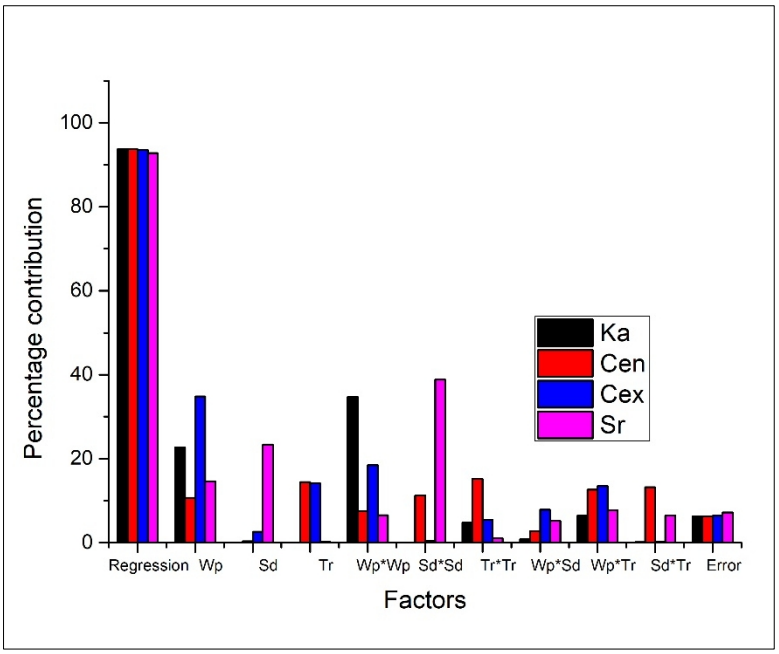

Figure 4 Factor contribution

Exit circularity once again illustrates pressure-controlled behavior with the contribution of water pressure and quadratic term being about 34.8% and 18.5% respectively which is higher than 53% and the traverse rate (14.1%) and the W_p x T_r interaction (13.5%) further modify the exit profile with the error contribution being low (6.4%). The single-factor domination is greatest with surface roughness, followed by standoff distance and its square term which collectively contribute some 23.4% and 38.8% respectively to the variation due to jet divergence and energy dispersal at higher nozzle heights; water pressure and the interaction terms used have secondary influence and the error term of 7.2% confirms the high level of reality consistency of the experiment. All this evidence shows that penetration-related responses (K_a and C_{ex}), the rate of traverse and standoff controls C_{en} and S_d is the major determinant of S_r.

In addition, the suitability of the regression models was also assessed by normal probability plots of the residuals of all response variables that can be found in Supplementary Figures S1-S4. The Pareto charts and the residual analyses, together, prove that there are specific dominant mechanisms controlling each AWJM response and proves the statistical validity of the elaborated regression models. In the case of K_a and C_{ex}, the

ARTICLE IN PRESS

pressure of water and the squares of this pressure become the most significant factors due to the key role of the jet energy and the nonlinear intensification of it in the determination of the kerf geometry and exit-profile formation. Entry circularity, on the contrary, shows a more spread out influence pattern with traverse rate standoff interaction and T_r^2 significant influencing factor, which means that inlet geometry is not influenced by one dominant factor. The most dominant parameter is the surface roughness where the standoff distance and S_d^2 represent majority of the effect, which is in line with surface deterioration caused by defocusing of the jet and the low concentration of abrasives at greater distances. In all answers, it is confirmed that the model assumptions are met: the residuals follow a normal distribution, they do not involve patterns, and they do not contain heteroscedasticity and autocorrelation. A combination of these diagnostics helps to conclude that the fitted models are statistically valid, physically interpretable and can be used to effectively represent the parameter response relationships driving performance at AWJM.

ARTICLE IN PRESS

Influence of AWJM process parameters on responses through 3D surface plots and 2D contour plots

The combined response surfaces in Figures 5–8 reveal that abrasive waterjet drilling performance in polycarbonate is governed by a delicate balance between jet coherence, energy distribution, and interaction time, which collectively dictate geometric accuracy and surface integrity. Across all responses, S_d consistently emerges as the most influential parameter, followed by W_p and T_r, though their effects vary depending on the quality metric considered.

In addition, to improve interpretation and the comprehension of interactions, relevant 2D contour plots are provided for each response (Figure 5-8 (d-f)). In these plots, the color gradient signifies the magnitude of the response variable, with cooler colors denoting lower values and warmer colors denoting higher values. This depiction facilitates a clear view of interaction areas and ideal parameter ranges.

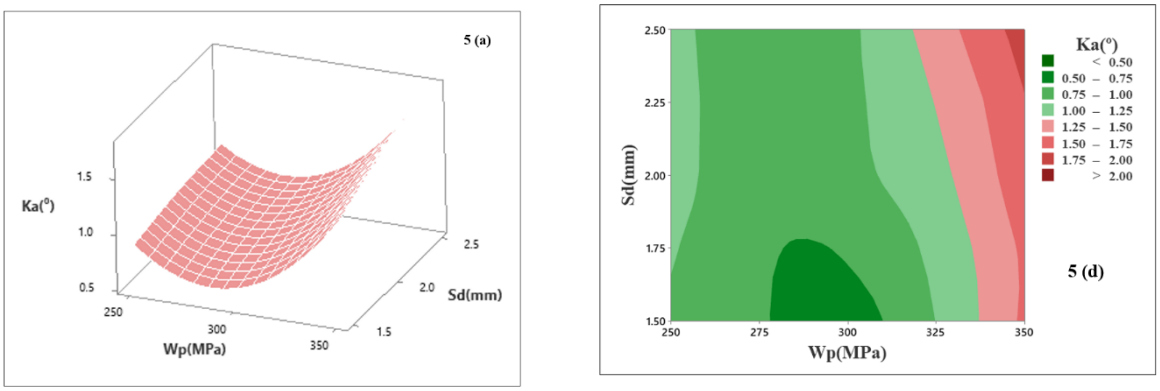

Figure 5(a) indicates that K_a is dominated by S_d which rises by 26% as S_d increases between 1.5 and 2.5 mm by progressive jet divergence and lower energy density at the exit. Water pressure is nonlinearly affecting the jet coherence, where mild W_p (300-325 MPa) stabilizes the jet coherence and minimizes the taper and the pressure high above (350 MPa) enhances K_a up to 2-3 times at larger S_d due to jet instability and particle fragmentation.

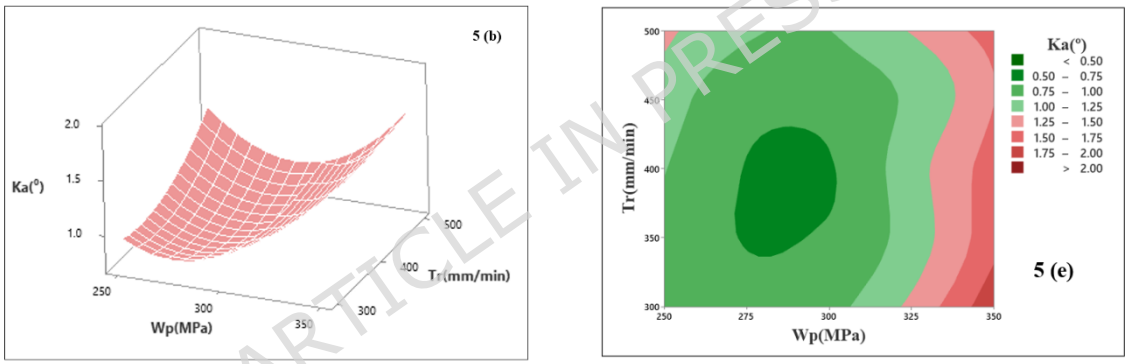

As illustrated in Figure 5(b), T_r further amplifies taper, with K_a increasing by 15% as T_r rises from 350 to 500 mm/min owing to shortened jet–material interaction time. At low T_r, excessive W_p sharply deteriorates kerf quality (K_a = 2.1°), whereas moderate W_p (300 MPa) suppresses taper even at higher T_r, yielding minimum K_a values (0.71°) and forming a distinct valley region where jet momentum and exposure time are optimally balanced. The combined influence of jet dispersion and reduced dwell time is evident in Figure 5(c), where increasing S_d at T_r = 300 mm/min raises K_a by 37%, confirming S_d as the dominant taper driver, while the maximum taper (1.5°) occurs under the synergistic action of high T_r and large S_d. Overall, Figures 5(a–c) identify low S_d, moderate W_p, and moderate T_r as the optimal parameter window for minimizing kerf taper.

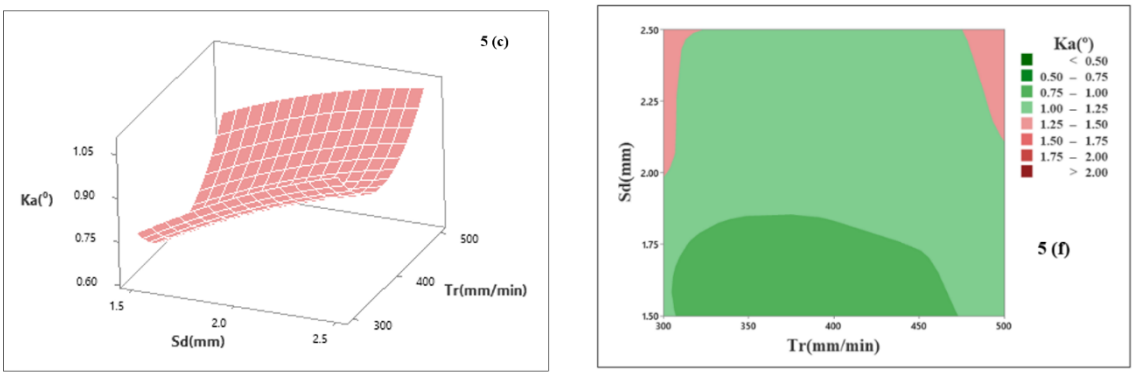

Figure 5 Influence of AWJM parameters on kerf angle

The contour graphs of Figure 5 (d-f) illustrate that the K_a diminishes with reduced S_d and moderate W_p. The closely spaced contour lines at elevated S_d distances indicate the significant impact of S_d distance on taper formation. The ideal region is identified at low S_d and moderate W_p, when jet coherence is enhanced, and taper is reduced. The impact of T_r is quite moderate but contributes to the overall interaction effect.

Figure 6(a) shows that water pressure is the most important factor with respect to entry circularity where C_{en} rises up to 150% as W_p increases between 250 and 350 MPa since erosion of the hole entry becomes more lateral. Standoff distance neutralizes this effect as C_{en} is decreased by 40-80% as S_d is increased by 0.5 to 2.5 mm jet spreading and decreased local impact.

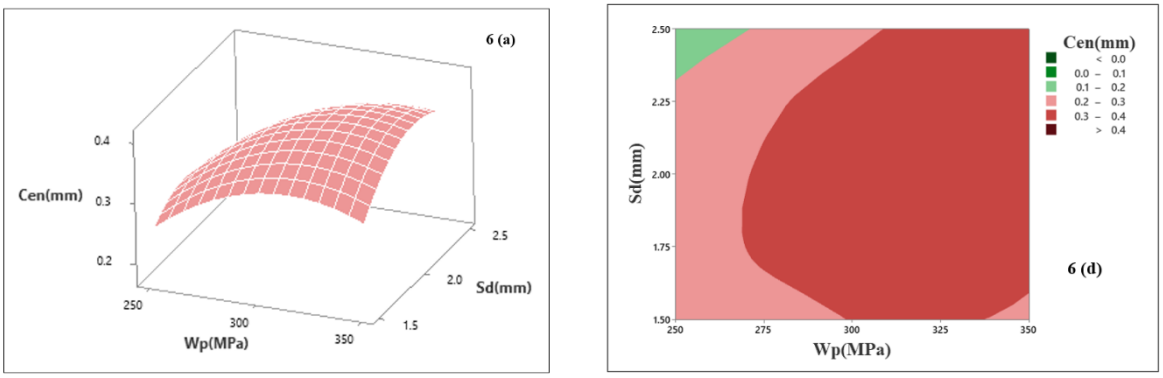

Because decreased dwelling time favors entry-edge widening over penetration, as indicated in Figure 6(b), traverse rate further increases C_{en} and this rate rises by 25-40%, as T_r rises between 300 and 500 mm/min. Further pressure (325 MPa or higher) brings C_{en} to a saturation plateau

ARTICLE IN PRESS

(0.33-0.39 mm), suggesting that further pressure increases abrasive dispersion primarily. The feed rapidity effect combined with the jet divergence effect is seen in the case of Figure 6(c) where the largest C_{en} is observed at large T_r and small S_d on the other hand, the greatest S_d with medium T_r produces the least entry circularity. In general, Figures 6(a-c) determine moderate W_p with higher S_d and restrained T_r as the good conditions to reduce entry circularity.

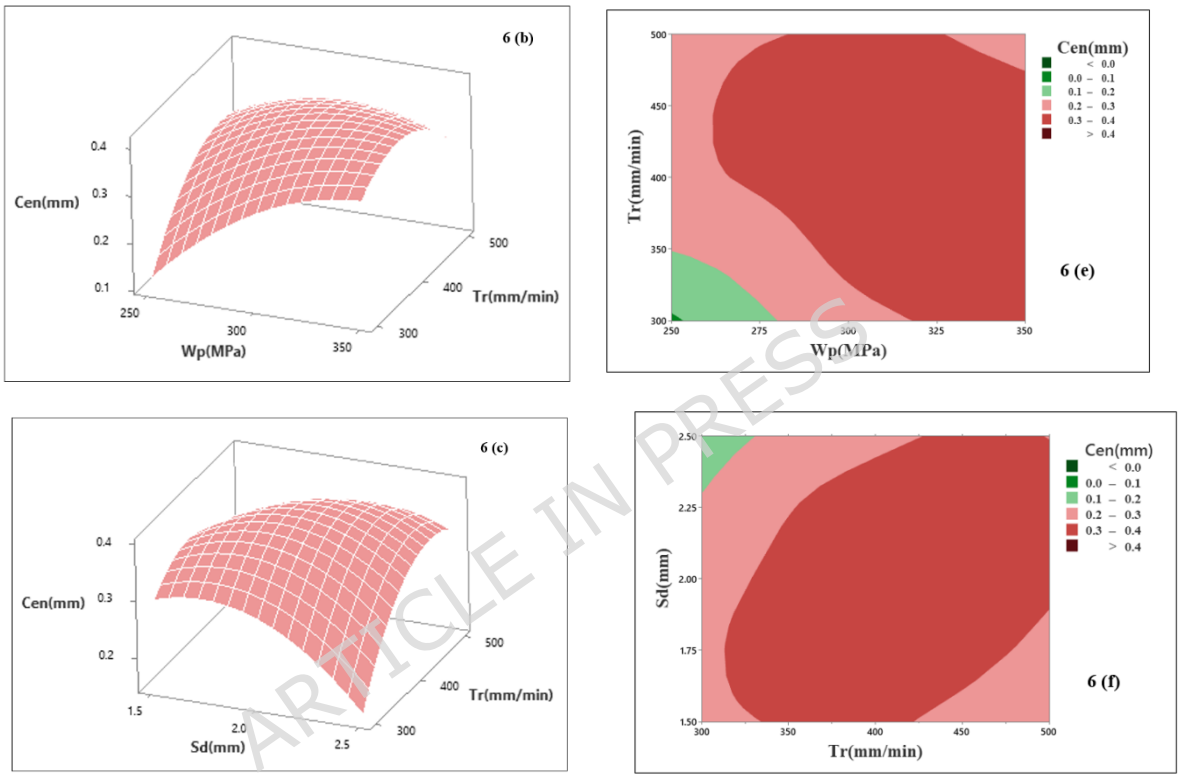

Figure 6 Influence of AWJM parameters on hole entry circularity

The contour plots of Figure 6 (d-f) indicate that the variation in hole entry circularity increases with rising water pressure. A comparatively stable region is noted at moderate Wp and reduced T_r, indicating enhanced entrance geometry under regulated jet impact conditions. The contour gradients suggest that W_p significantly affects C_{en}.

Figure 7(a) shows that exit circularity is nonlinearly dependent on water pressure, peaking at id-range pressures (300-325 MPa), and low pressure as well as excessive pressure decrease ircularity as the jet is not penetrating enough or is not stable. The secondary but steady impact of

ARTICLE IN PRESS

standoff distance is to reduce C_{ex} by a factor of about 14% as S_d is raised between 1.5 and 2.5 mm due to greater jet dispersion prior to the emergence of the jet exit.

The beneficial role of traverse rate is evident in Figure 7(b), where increasing T_r from 300 to 500 mm/min improves C_{ex} by 39%, likely by limiting uneven circumferential erosion during prolonged exposure. The combined effect of jet focus and exposure time is captured in Figure 7(c), which shows that moderate T_r with low S_d yields the highest exit circularity, whereas low T_r and large S_d produce the poorest exit geometry. Collectively, Figures 7(a–c) indicate that moderate W_p, moderate-to-high T_r, and low S_d provide the most stable exit profiles.

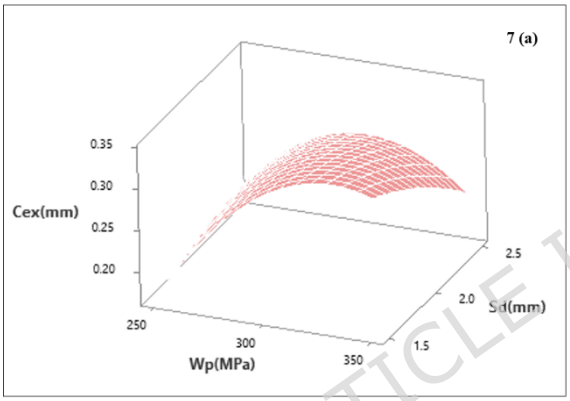

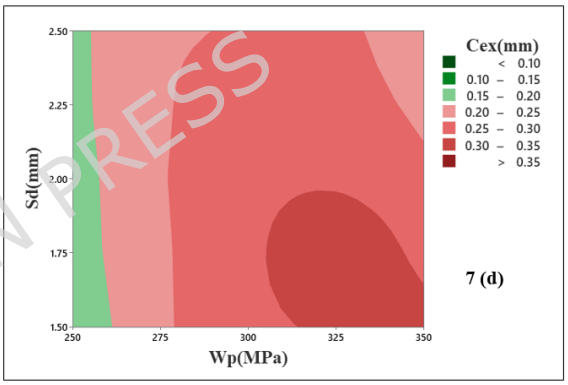

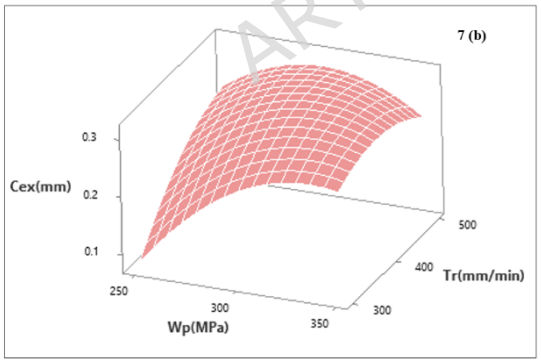

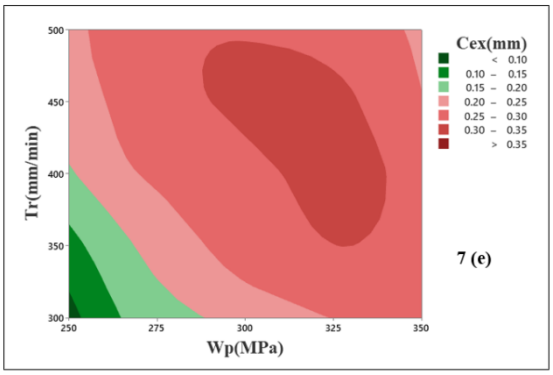

ARTICLE IN PRESS

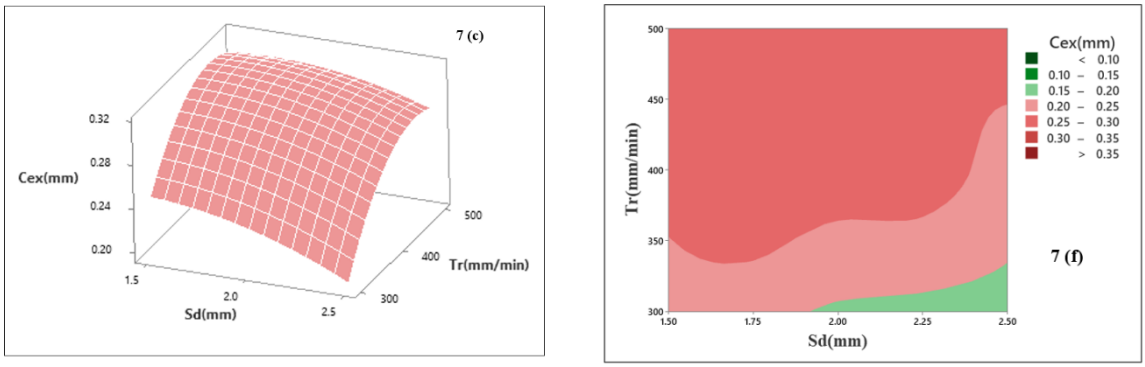

Figure 7 Influence of AWJM parameters on hole exit circularity

The contour plots indicate that exit circularity increased at moderate W_p and moderate T_r pace. At greater S_d, the contour lines become more concentrated, signifying degradation resulting from elevated jet divergence prior to departure. The ideal parameter range is confined to a specific pressure range, underscoring the necessity for stability in penetration energy.

Figure 8(a) demonstrates that standoff distance is the dominant factor influencing surface roughness, with S_r increasing by 100% as S_d rises from 1.5 to 2.5 mm due to jet divergence and reduced micro-cutting effectiveness. Water pressure modifies this trend nonlinearly, where moderate pressures (300–325 MPa) minimize S_r, while excessive pressure (350 MPa) increases roughness by 40–60% because of jet instability and micro-chipping. As shown in Figure 8(b), traverse rate further degrades surface quality, increasing S_r by 9–15% as T_r rises from 300 to 500 mm/min owing to shortened dwell time and incomplete abrasive action.

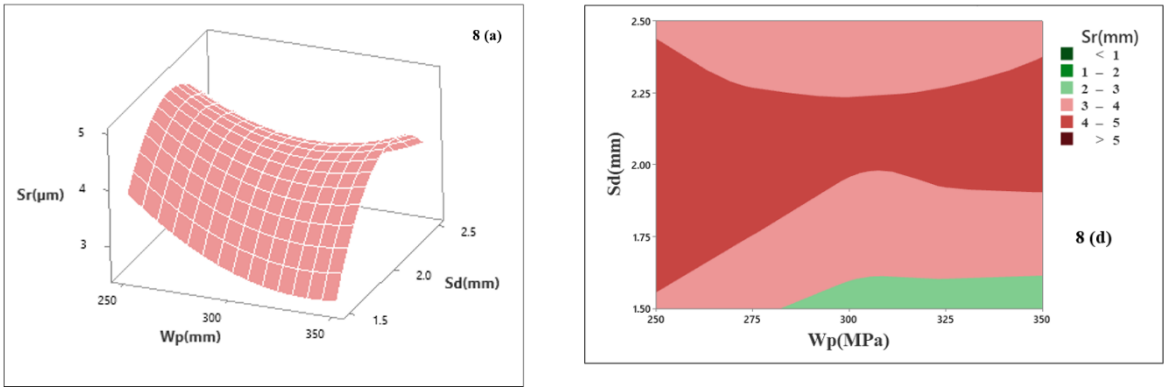

ARTICLE IN PRESS

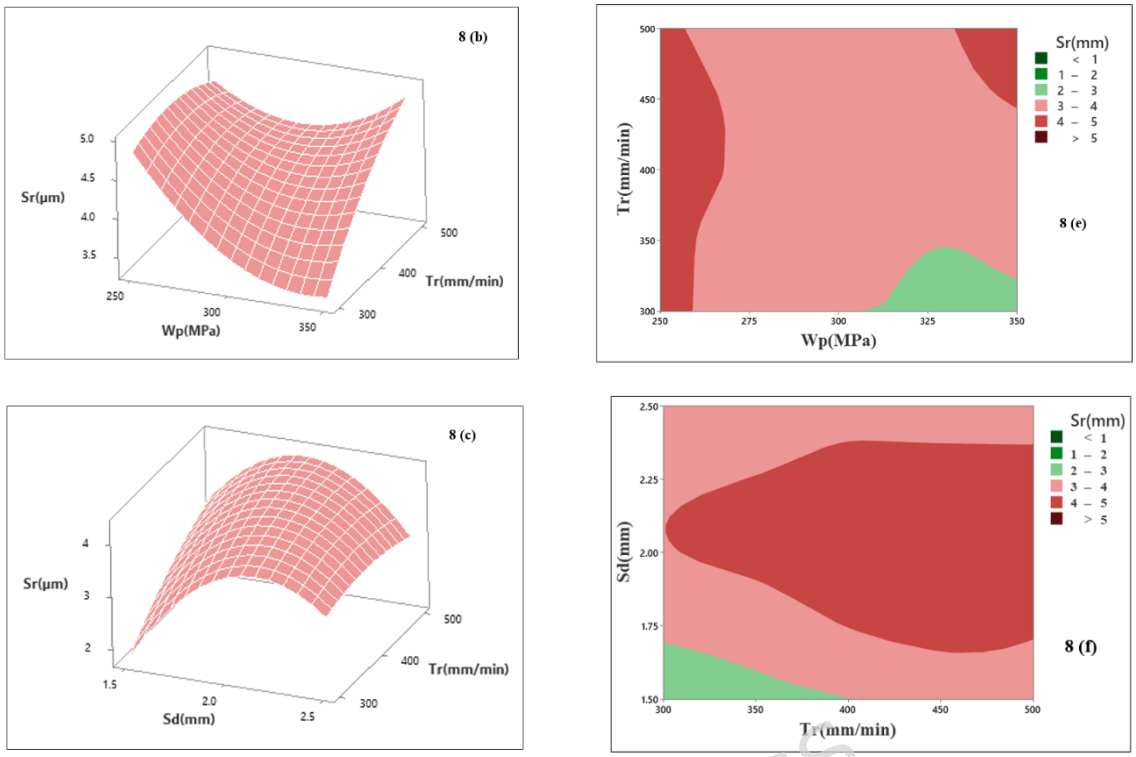

Figure 8 Influence of AWJM parameters on surface roughness

The compounded effect of jet dispersion and limited interaction time is evident in Figure 8(c), where the highest S_r occurs at high T_r combined with large S_d, while the smoothest kerf walls are obtained at low S_d, moderate W_p, and low-to-moderate T_r. Overall, Figures 8(a–c) identify a clear surface-finish optimum governed by jet stability and exposure time.

The contour representation of Figure 8 (d-f) indicates that surface roughness increases with an increase in S_d and a higher T_r. The minimal S_r values are observed with moderate W_p and low S_d, signifying stable erosion conditions. The contour distribution verifies that preserving jet stability is crucial for enhancing surface quality.

Machine learning approach

In order to overcome the high nonlinearity of AWJM drilling, machine learning approach based on data was applied to determine credible input to output correlations. Structured data splitting was initially used to condition experimental results obtained after systematically designed drilling trials to facilitate a stable learning. W_p, S_d and T_r have been taken as model input and K_a, C_{en} and C_{ex} circularity, and S_r have been taken as

ARTICLE IN PRESS

response variables. In a manner of independent training, ABR, XGB, DT, and RF models were trained in order to capture the underlying jet-material interaction mechanisms. The coefficient of determination, and error-based measures were used to compare the model performance to determine the predictor that was most accurate in comparison to MLRM. The choice of the ML model was followed by the combination with the evolutionary optimization algorithms, and the optimal drilling parameters were tested experimentally to assure the predictive accuracy and consistency of the processes.

Hyperparameter tuning and cross validation

To achieve systematic optimization, specific hyperparameter ranges were developed for each machine learning approach (DT, RF, ABR, and XGB) prior to training. The ranges were established with algorithmic stability in mind, as well as generally reported effective intervals in regression-based modeling of structured experimental datasets. Discrete hyperparameters (for example, tree depth, minimum sample split) were drawn from integer uniform distributions, whereas continuous hyperparameters (for example, learning rate, subsample ratio) were drawn from uniform distributions. Establishing constrained yet adequately vast search domains mitigates underfitting from overly restrictive parameters and overfitting resulting from excessively intricate model architectures. The whole search space is represented in Table 4(a).

ARTICLE IN PRESS

Table 4(a) Hyperparameter search space setting

Model	Hyperparameter search space
Decision Tree	'max_depth': randint(1, 20), # Maximum depth of the tree,

ARTICLE IN PRESS

	'min_samples_split': randint(2, 20), # Minimum number of samples required to split an internal node, 'min_samples_leaf': randint(1, 20), # Minimum number of samples required to be at a leaf node
Random Forest	'n_estimators': randint(10, 500), 'max_depth': randint(5, 20), 'min_samples_split': randint(2, 10), 'min_samples_leaf': randint(1, 4)
AdaBoost Regressor	'n_estimators': randint(50, 200), # Number of weak learners, 'learning_rate': uniform(0.01, 1.0) # Contribution of each weak learner
Extreme Gradient Boosting	'max_depth': randint(3, 10), # Maximum tree depth, 'learning_rate': uniform(0.01, 1.0), # Learning rate, 'n_estimators': randint(50, 200), # Number of trees, 'gamma': uniform(0, 0.5), # Minimum loss reduction required to make a further partition on a leaf node ,'subsample': uniform(0.5, 0.5), # Subsample ratio of the training instances, 'colsample_bytree': uniform(0.5, 0.5), # Subsample ratio of columns when constructing each tree

Hyperparameter optimization was conducted by randomized search with 50 iterations for each model. In each iteration, a randomly chosen group of hyperparameters was selected from the established search space and assessed using 5-fold cross-validation. Considering a dataset of 125 experimental observations, 5-fold cross-validation was deemed a statistically suitable balance between bias and variance. The dataset was

ARTICLE IN PRESS

randomly divided into five equal subgroups, each containing 25 samples. In each iteration, four folds (100 samples) were utilized for model training, while the remaining fold (25 samples) served for validation. The method was executed five times, with each fold utilized once as the validation set. Employing cross-validation in hyperparameter tuning mitigates bias from a singular train-test partition and enhances resilience to overfitting.

The model's predictive performance was assessed by calculating the mean and standard deviation of performance measures across five cross-validation stages. The coefficient of determination (R^2) was employed to assess the predictive ability. The R^2 values for the five iterations ranged from 92% to 96%. The average R^2 obtained after 5-fold cross-validation was 9% with standard deviation of 0.02, considered a more dependable measure of model generalization than a single train-test split, as outlined in Table 4(b).

Table 4(b) 5-fold cross validation results of the RF model

Iteration	Training folds	Validation fold	R^2
1	2,3,4,5	1	0.93
2	1,3,4,5	2	0.95
3	1,2,4,5	3	0.94
4	1,2,3,5	4	0.96
5	1,2,3,4	5	0.92
Mean ± Standard deviation			0.94 ± 0.02

ARTICLE IN PRESS

Hyperparameter tuning using random search led to response-specific optimum model configurations, as shown in Table 4(c). Random Forest model showed overall good results as geometrical responses were always better as the trees were deeper and the node-splitting parameters optimized to well represent the nonlinear jet-material interactions. Conversely, surface roughness was more sensitive to nonlinear and was better represented by the XGBoost model that optimized the learning rate, depth, and feature sampling features. This custom tuning plan guaranteed better generalization potential and predictive strength of all AWJM drilling responses, which constitutes a sound basis of the further optimization and validation.

Table 4(c) Tuned hyperparameter settings

ARTICLE IN PRESS

Response	Selected ML model	Tuned hyperparameters
Kerf angle	Random Forest	Max depth = 16, Number of trees = 469
Entry circularity	Random Forest	Max depth = 12, Min samples per leaf = 3, Min samples per split = 7
Exit circularity	Random Forest	Max depth = 14, Min samples per leaf = 2, Min samples per split = 6
Surface roughness	XGBoost	Learning rate = 0.302, Max depth = 9, Estimators = 100, Colsample by tree = 0.806, Gamma = 0.070

A series of quantitative statistical indicators, such as the coefficient of determination (R^2), Mean Square Error (MSE), Root Mean Square Error (RMSE), Mean Absolute Error (MAE), Relative Standard Error (RSE), Relative Absolute Error (RAE), and Correlation Coefficient (CC), were used to evaluate the predictive performance of the machine learning models created for AWJM of polycarbonate. These metrics offer an unbiased assessment of the degree to which the predicted values correspond with the responses that were observed during the experiment. Greater predictive fidelity is generally indicated by higher R^2 and CC values along with lower error values. The MLRM, which serves as a conventional reference method but is intrinsically limited when nonlinear or interaction effects dominate the behavior of the machining process, was used as the benchmark for all ML models.

The results provided in Table 5 and comparison of ML models based on R^2 and RMSE depicted in Figure 9, demonstrate substantial differences among the ML models in predicting the four AWJM responses for K_a, C_{en}, C_{ex}, and S_r. For K_a, the RF model delivered the most accurate predictions, achieving an R^2 of 0.9449**,** MSE of 0.0385**,** and RMSE of 0.1962**.** These values were significantly lower than those obtained using XGB (RMSE = 0.2162) and ABR (RMSE = 0.3328). The RSE (0.0550) and RAE (0.2227) of RF further highlight its ability to model the nonlinear flow characteristics, abrasive energy distribution, and jet-material interaction mechanisms that govern kerf taper formation.

Table 5 Performance comparison of ML algorithm with MLRM

ARTICLE IN PRESS

Response	ML	R^2	MSE	RMSE	MAE	RSE	RAE	CC
K_a	ABR	0.841585	0.110787	0.332847	0.279122	0.158415	0.43598	0.933841
	XGB	0.933164	0.046741	0.216197	0.14397	0.066836	0.224876	0.967115
	DT	0.892714	0.07503	0.273916	0.196866	0.107286	0.307499	0.945118
	RF	0.944949	0.0385	0.196213	0.142557	0.055051	0.222669	0.978126
	MLRM	0.891329	0.070544	0.265601	0.216076	0.033565	0.178478	0.944102
C_{en}	ABR	0.784191	0.002551	0.050509	0.038919	0.215809	0.447962	0.88765
	XGB	0.79313	0.002446	0.049452	0.035962	0.20687	0.41393	0.891617
	DT	0.715114	0.003368	0.058033	0.042332	0.284886	0.487251	0.846663
	RF	0.82679	0.002048	0.04525	0.030913	0.17321	0.355817	0.912185
	MLRM	0.761799	0.004558	0.067515	0.049531	0.041654	0.174606	0.872811
C_{ex}	ABR	0.701994	0.002944	0.05426	0.039737	0.298006	0.516114	0.841754
	XGB	0.734993	0.002618	0.051167	0.036098	0.265007	0.468858	0.861474
	DT	0.763502	0.002336	0.048337	0.030904	0.236498	0.401397	0.878529
	RF	0.822484	0.001754	0.041878	0.025765	0.177516	0.334642	0.90753
	MLRM	0.585829	0.007719	0.087859	0.06636	0.090308	0.269147	0.765395
S_r	ABR	0.824697	0.499603	0.706826	0.579475	0.175303	0.42882	0.926873
	XGB	0.928182	0.204676	0.452411	0.248301	0.071818	0.183746	0.965046
	DT	0.802253	0.563568	0.750712	0.557321	0.197747	0.412425	0.896507
	RF	0.914307	0.244221	0.494187	0.345623	0.085693	0.255766	0.961951
	MLRM	0.764856	0.159274	0.399092	0.298519	0.011839	0.084128	0.874561

In the prediction of C_{en}, RF once again had the best results, with an MAE of 0.0309, an RMSE of 0.0453, and a R^2 of 0.8268. When compared to ABR and XGB, RF always had a stronger correlation and fewer prediction errors. RF's ensemble-based architecture, which includes many decision routes and accurately reflects the erosion dynamics happening in the entry zone, where the abrasive-laden jet is most stable and coherent, is what makes it better at generalizing.

ARTICLE IN PRESS

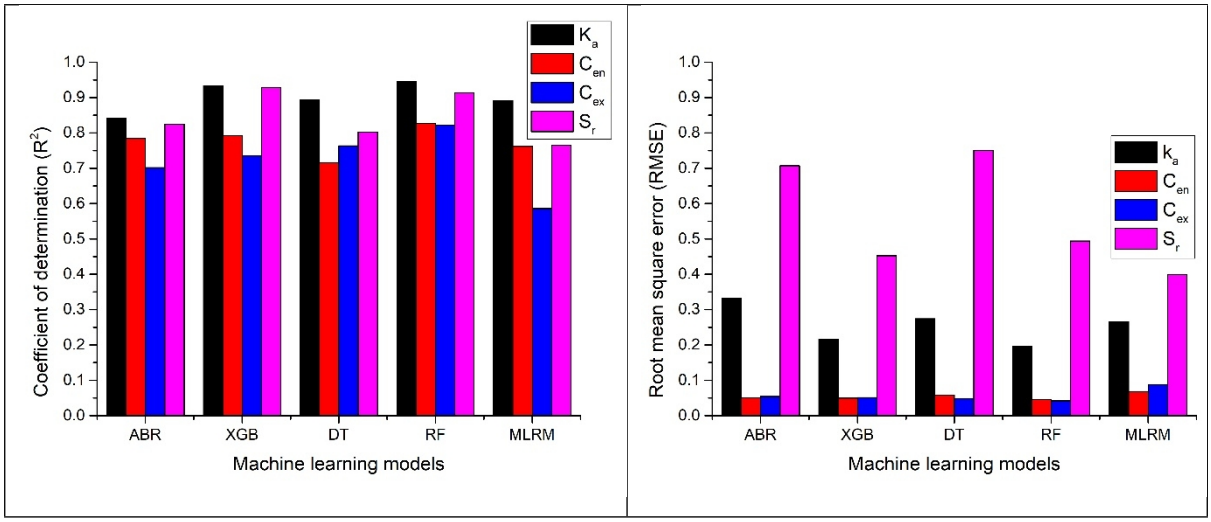

Figure 9 Comparison of ML model based on performance metrics

The RF model kept its top performance for C_{ex}, with a R^2 value of 0.8225, an MSE of 0.001754, and the lowest RMSE (0.04188) of all the models studied. The MAE of RF (0.02577) was also much lower than the MAE of DT, XGB, and ABR. These results show that RF can describe the random and unstable erosion processes that happen on the exit side, where the jet tends to lose coherence and turbulence effects become stronger.

A similar trend was confirmed for S_r, where RF also emerged as the superior model. After parameter reallocation, RF achieved an R^2 of 0.9143**,** MSE of 0.2442**,** and RMSE of 0.4942**,** outperforming all other tested algorithms**.** The RSE (0.08569) and RAE (0.2558) obtained for RF indicate that it effectively modelled the multi-scale surface irregularities resulting from abrasive impacts, micro-cutting actions, and localized plastic deformation. Ensemble averaging within RF reduces noise propagation and enhances its ability to reproduce the complex topographical variations characteristic of AWJM processed polymer surfaces.

RF consistently did better than the typical MLRM in all four cases. The MLRM had lesser predictive strength, as evidenced by its modest R^2 values (0.8913 for K_a, 0.7618 for C_{en}, 0.5858 for C_{ex}, and 0.7649 for S_r). Because MLRM is linear, it has trouble understanding nonlinear input-output interactions. On the other hand, RF's ensemble learning method makes predictions that are more accurate and reliable. RF reduced RMSE values

ARTICLE IN PRESS

by around 49–70% in comparison to MLRM, indicating its superior capability in predicting AWJM behavior.

While the statistical metrics confirm the superior predictive accuracy of the Random Forest model, its effectiveness can also be interpreted in relation to the underlying erosion mechanics of AWJM in polycarbonate. Polycarbonate removal under abrasive waterjet drilling is governed by ductile deformation, localized plastic flow, and stochastic abrasive impact distribution, leading to strong nonlinear and interaction-driven behavior among water pressure, standoff distance, and traverse rate. The ANOVA results indicate significant quadratic and interaction effects, particularly for kerf angle and circularity responses.

Random Forest is well suited to capture such piecewise nonlinear relationships because it partitions the parameter space into multiple locally adaptive regions and aggregates their predictions through ensemble averaging. This structure reduces variance caused by experimental noise and jet instability while preserving complex interaction patterns. In contrast, single-tree models are more sensitive to variance, and boosting-based methods may amplify localized fluctuations. Therefore, RF's ensemble-based variance reduction and interaction modeling capability align closely with the stochastic and nonlinear jet–polymer erosion behavior, explaining its consistent superiority across geometric and surface integrity metrics.

The results affirm that the RF model is the most efficient and dependable approach for forecasting all principal AWJD responses: K_a, C_{en}, C_{ex}, and S_r. The consistent performance of RF in geometric and surface-quality outputs underscores its appropriateness for use into intelligent machining systems. The significant quantitative enhancements underscore the promise of machine learning-based modeling for process monitoring, optimization, and decision-making in abrasive waterjet machining of polymeric materials.

ARTICLE IN PRESS

Evolutionary optimization algorithmic approach

The four evolutionary algorithms applied in the current work were BBO, PSO, SSO, and TWO which were used to find the optimal AWJM parameters using the multi-indicator evaluation model presented in Table 6. Every algorithm was repeated 21 times individually and the best solution of each run was selected on the overall Objective Value (OV) in Supplementary Tables S5-S8. The optimization process also involved several performance metrics such as Convergence Iteration (CI), Convergence Value (CV), Inter-Generated Distance (IGD), Diversity (Div), Spacing (SP), and Hypervolume (HV) and all the indicators had equal weight.

To assess the comprehensive efficacy of each optimization procedure across various machining responses K_a, C_{en}, C_{ex}, and S_r a single composite objective value was calculated utilizing Deng's similarity-based aggregation method. Given that all responses denote minimization-type objectives, each response value was normalized as follows:

$$r_i = f_i(\min) / f_i, \quad i = 1, 2, 3, 4$$

Where:

f_i = observed value of the ith machining response

f_i (min) = minimum value of the ith response among all compared algorithms

r_i = normalized performance score of the ith objective

i = index corresponding to K_a, Ce_n, C_{ex}, and S_r

This transformation standardizes all objectives to a dimensionless maximizing scale such that:

$$0 < r_i \leq 1$$

Assuming equal importance of all objectives, uniform weighting was applied:

$$w_i = 1 / m$$

Where:

w_i = weight assigned to the ith objective

m = total number of objectives (here, m = 4)

The overall performance value (DV) was then calculated as:

$$DV = \Sigma (w_i r_i), \quad i = 1 \rightarrow m$$

ARTICLE IN PRESS

Where:

DV = composite single-objective performance value

The multi-indicator aggregation technique by Deng was then used to find the global ranking of each algorithm, the higher the Deng's value (DV), the better the optimization behavior. The computed DV values were used for algorithm ranking and are presented in Tables 6 and 7. The best combination of machining parameters W_p, S_d, and T_r and the best responses, K_a, C_{en}, and C_{ex} circularity, and S_r were determined based on the maximum OV attained by each algorithm. The convergence iteration and the optimum value and condition of all the four algorithms are outlined in the supplementary Tables S9 -S12.

The convergence behavior analysis during each of the runs revealed that the four algorithms differed significantly in their levels of performance. Most responses (K_a, C_{en}, C_{ex} and S_r) stabilized the fastest with SSO, most frequently in 1-5 iterations. This implies that it could exploit the situations promptly and did not swing very widely. BBO and PSO demonstrated characteristic features of moderate convergence, which typically applied at 10 to 90 iterations, according to the response variable. More iterations were required to stabilize TWO, with C_{ex} and S_r frequently requiring over 85-100 iterations. This indicates that it was more exploratory in search. In addition, the Pareto front curves in Figures 10-13 clearly highlight the differences in the optimization effectiveness of the discussed approaches. Of the four methods, SSO always yields a smaller and evenly spaced set of non-dominated solutions that are closer to the ideal zone, whereby kerf angle and circularity deviations at entry and exit are reduced to the minimum as well as the surface roughness. The elegant and small Pareto fronts produced with the help of SSO show a steady convergence and effective handling of contrary goals.

ARTICLE IN PRESS

ARTICLE IN PRESS

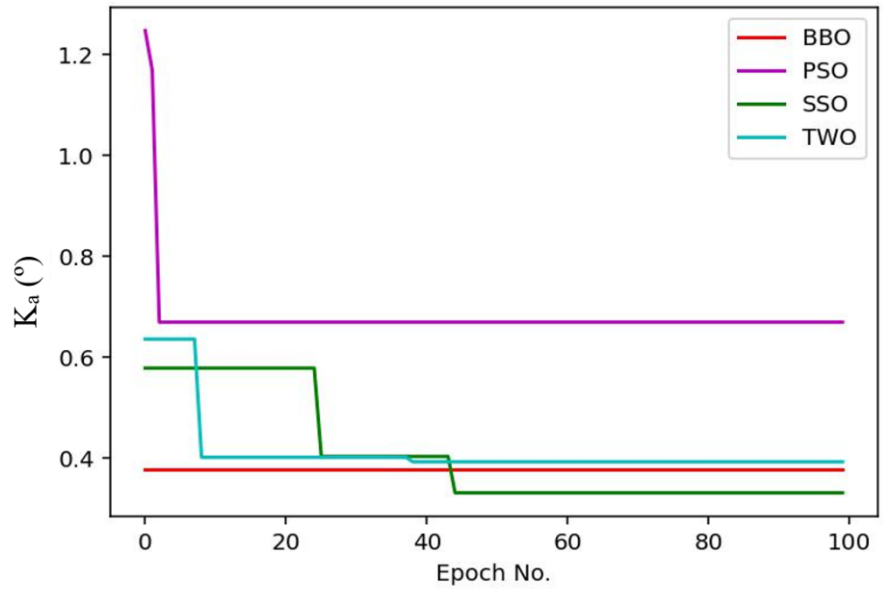

Figure 10 Pareto front for K_a

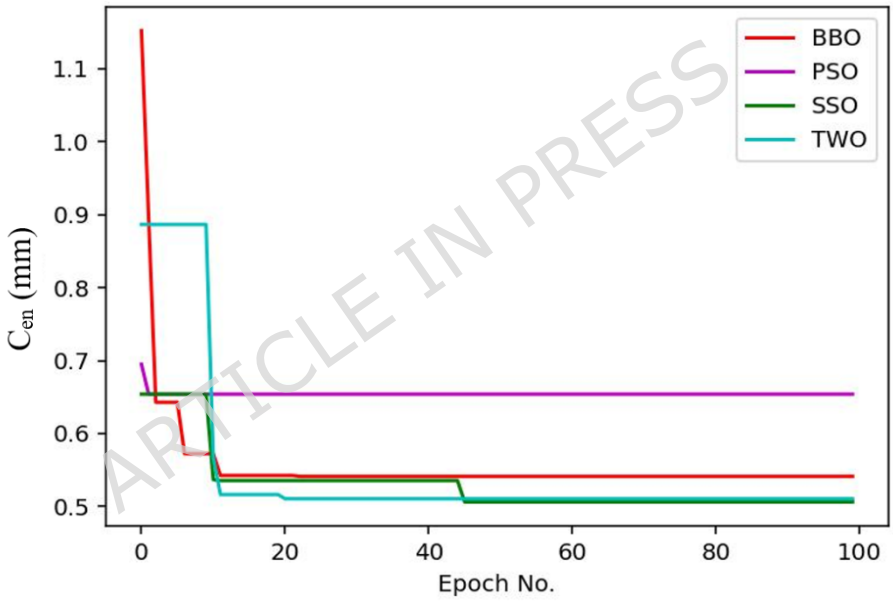

Figure 11 Pareto front for C_{en}

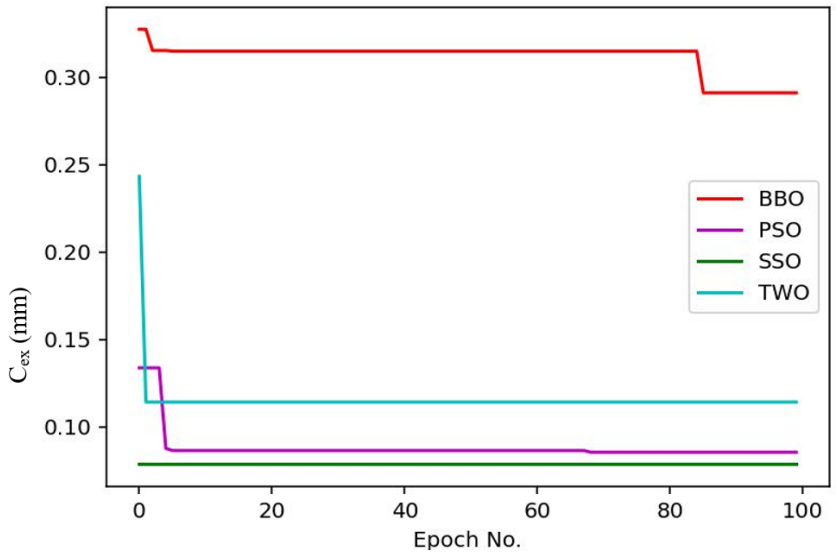

Figure 12 Pareto front for C_{ex}

BBO and PSO exhibit similar and less dependable performance. There is more width and less concentration in the low-circularity region of their Pareto fronts with a slower convergence to a high-precision solution. Even though both algorithms have the ability to explore a large search space, the sets of solutions have a smaller number of dominating points that simultaneously meet all reduction goals, particularly with respect to circularity-related responses.

On the other hand, TWO is highly diverse in the Pareto fronts. Although it sometimes has extreme solutions, which have low objective values, they are scattered and lack continuity. This action indicates strong exploration and limited exploitation leading to an unstable convergence when a large number of precision-related objectives are considered.

Table 6 shows the optimal process parameters and the responses of AWJM to these parameters based on the maximum value of Deng of each algorithm. The close observation of the performance criteria, convergence, computational power, and general objective values show that SSO is the most reliable and the most effective evolutionary algorithm to optimize the AWJM process.

ARTICLE IN PRESS

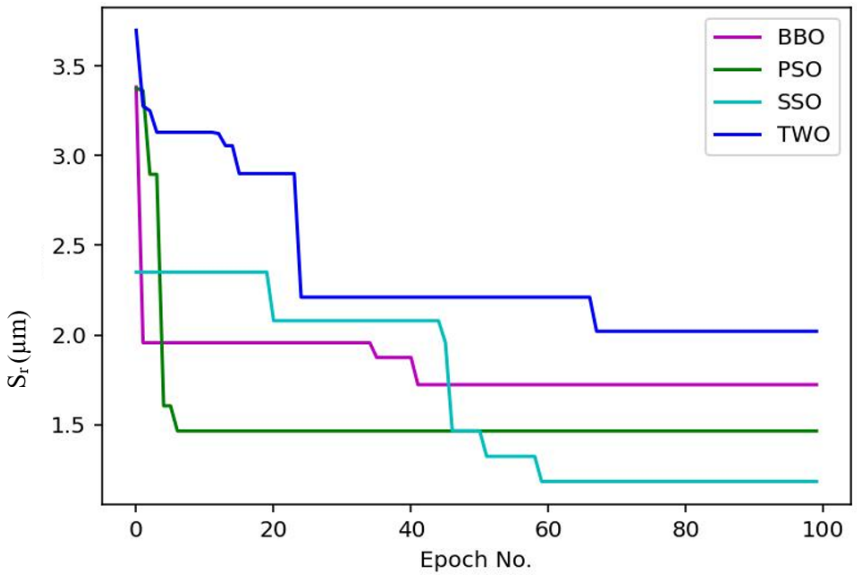

Figure 13 Pareto front for S_r

Table 6 Optimum process parameters and their associated responses

Algorithm	W_p (MPa)	T_r (mm/min)	S_d (mm)	K_a (°)	C_{en} (mm)	C_{ex} (mm)	S_r (µm)	(DV)
BBO	305.63	341.04	1.605	1.090	1.052	0.127	3.000	0.598807
PSO	300.38	428.13	2.051	0.728	0.744	0.204	5.390	0.576012
SSO	250	300	1.50	0.597	0.717	0.079	2.350	0.621896
TWO	265.66	306.05	2.459	0.436	0.527	0.314	1.182	0.589038

ARTICLE IN PRESS

The Friedman test was performed to examine the significance of the ranking of the four optimization algorithms in all the variables statistically. The probability values and rankings have been shown in Table 7. Comparative performance analysis shows that there exists clear differences in the performance of the optimization techniques as far as computational efficiency, convergence behavior, and quality of solutions are concerned. The metric of the computational time shows a statistically significant difference ($p = 0.020883$), and BBO took the shortest time to

ARTICLE IN PRESS

complete the optimization process, where TWO always required the most time in a series of experiments. After analyzing convergence-related indicators, including convergence iterations of kerf angle, top and bottom circularity, and the surface roughness, SSO had the lowest mean values, which indicated a faster and more reliable convergence. This tendency is also supported by convergence value measures of all the responses, where SSO was always rated first (highlighted in bold), which means that it is better at the solution correctness and stability measure.

Table 7 Performance of algorithms based on their metrics through Friedman test

Metrics	Probability	BBO	PSO	SSO	TWO
Time	0.020883	1.952381	2.285714	2.619048	3.142857
CI_K_a	0.071726	2.5	2.785714	1.928571	2.785714
CI_C_{en}	6.65E-05	3.119048	2.690476	1.714286	2.47619
CI_C_{ex}	8.77E-09	2.047619	2.190476	1.857143	3.904762
CI_S_r	2.98E-08	2.595238	2.428571	1.309524	3.666667
CV_K_a	2.36E-13	2.047619	2.952381	**1**	4
CV_C_{en}	1.34E-13	2	3	**1**	4
CV_C_{ex}	1.34E-13	2	3	**1**	4
CV_S_r	1.34E-13	2	3	**1**	4
OV	1.34E-13	2	3	**1**	4
IGD		0.237632	0.485084	0.113637	0.668413
Div		2.254443	4.770776	1.827896	6.151466
SP		0.079925	0.327691	0.121835	0.239784
HV		0.284	0.143	0.313	0.34
DV		0.598807	0.576012	**0.621896**	0.589038

ARTICLE IN PRESS

The same tendency is observed in the total objective value, where SSO outperforms BBO, PSO, and TWO therefore confirming that it has the ability to offer optimal solutions in a balanced manner. In terms of multi-objective distribution properties, SSO achieved the lowest IGD value of 0.1136, that is, almost equal to the true Pareto front, and the most homogeneous solution spacing with the least spacing value of 0.1218. Although TWO illustrated a better level of exploration, as indicated by the highest variety and hypervolume metrics, its responses were less coherent and required a longer time of calculation. Overall, contrary to BBO, PSO,

ARTICLE IN PRESS

and TWO, which demonstrated clear advantages, SSO performed better than other measures in most of the vital parameters, particularly regarding the convergence efficiency, the quality of solutions, and stability.

The Friedman test revealed statistically significant differences among the evaluated algorithms across many performance measures ($p < 0.05$). Nonetheless, the Friedman test does not ascertain which particular algorithm pairs show significant differences. Consequently, a Nemenyi post-hoc analysis was executed to enable pairwise comparisons. The Nemenyi test is suitable when multiple algorithms are assessed throughout the same set of trials and the Friedman test eliminates the null hypothesis. This study assessed four algorithms (BBO, PSO, SSO, and TWO) across 21 trials. Algorithms were rated by each statistic within each trial, and average ranks were calculated.

For k=4 algorithm, and N=21 trials, the critical difference (CD) at a significance level of $\alpha=0.05$ was calculated as:

$$CD = 2.569\sqrt{\frac{4(4+1)}{6*21}} = 1.02$$

Two algorithms were deemed considerably different if the absolute difference in their average ranks surpassed 1.02. Tables 8 and 9 display the average ranks for all selected algorithms and the pairwise comparisons, respectively. SSO attained the highest rank (1.000), succeeded by BBO (2.048), PSO (2.952), and TWO (4.000).

Table 8 Algorithm average rank

Algorithm	Average Rank
SSO	**1.000**
BBO	2.048
PSO	2.952
TWO	4.000

Table 9 Pairwise rank difference

Algorithm pair	Rank difference	Significance
SSO VS BBO	1.048	Yes
SSO VS PSO	1.952	Yes
SSO VS TWO	3.000	Yes

ARTICLE IN PRESS

BBO VS PSO	0.905	No
BBO VS TWO	1.952	Yes
PSO VS TWO	1.048	Yes

In multiple statistically significant parameters, SSO consistently attained the lowest (optimal) average rank. The rank disparities between SSO and TWO surpassed the CD threshold in several convergence and constraint-related metrics, affirming statistically substantial superiority. BBO and PSO often demonstrated rank discrepancies within the CD range, indicating similar performance across various measures. While TWO exhibited competitive behavior in specific metrics, it typically ranked lower in managing constraints and convergence efficacy.

Overall, the Nemenyi post-hoc analysis reveals the precise algorithm pairings responsible for the significant Friedman test findings, confirming that the observed statistical differences are mostly due to SSO's persistent superiority across many assessment criteria.

Experimental validation

In order to confirm the practical feasibility of the suggested optimization framework, the confirmatory drilling experiments were performed in the most favorable process conditions that were determined using the combined machine learning-optimization strategy. To validate the experimentally, the drilling trials with the best process parameters were repeated 5 times to ascertain process repeatability and robustness. Moreover, the response characteristics, each of the kerf angle, entry and exit circularity as well as the surface roughness were measured three times in each of the drilled holes and a means value was obtained which was to be compared with the predicted results. The results of the measurement are presented in Table 10 and Figure 14. This repetition scheme reduces the effects of random process variations and measurement errors to have a dependable evaluation of the consistency and reproduction of the recommended machine learning-optimization scheme. The holes are measured with high-precision digital microscope of

ARTICLE IN PRESS

model AM4515 whose magnification is 20X- 220X and the hole circularity was measured using CMM.

Table 10 Measurement of hole diameter using digital microscope

Trail No.	Hole entry diameter (mm)	Hole exit diameter (mm)	Hole entry circularity (mm)	Hole exit circularity (mm)
1	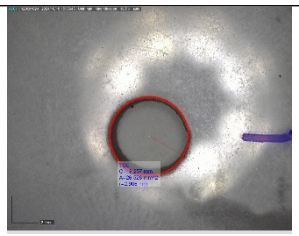	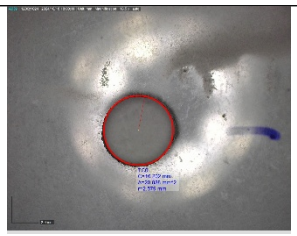	0.689	0.084
2		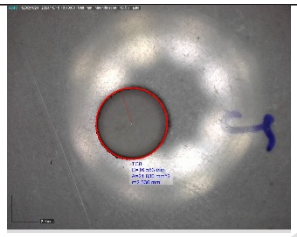	0.683	0.080
3	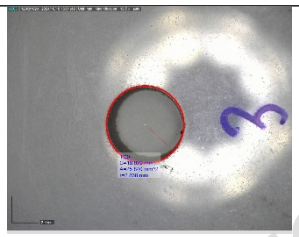		0.695	0.082
4	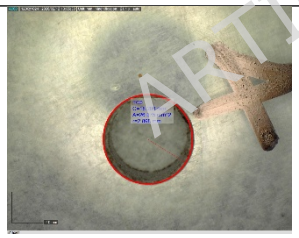		0.685	0.082
5	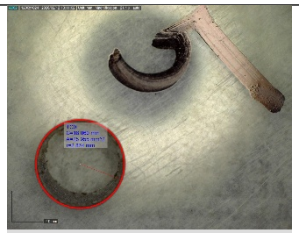	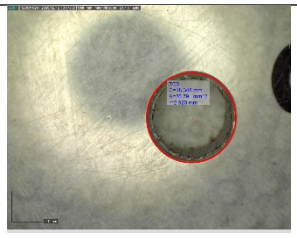	0.691	0.083

ARTICLE IN PRESS

ARTICLE IN PRESS

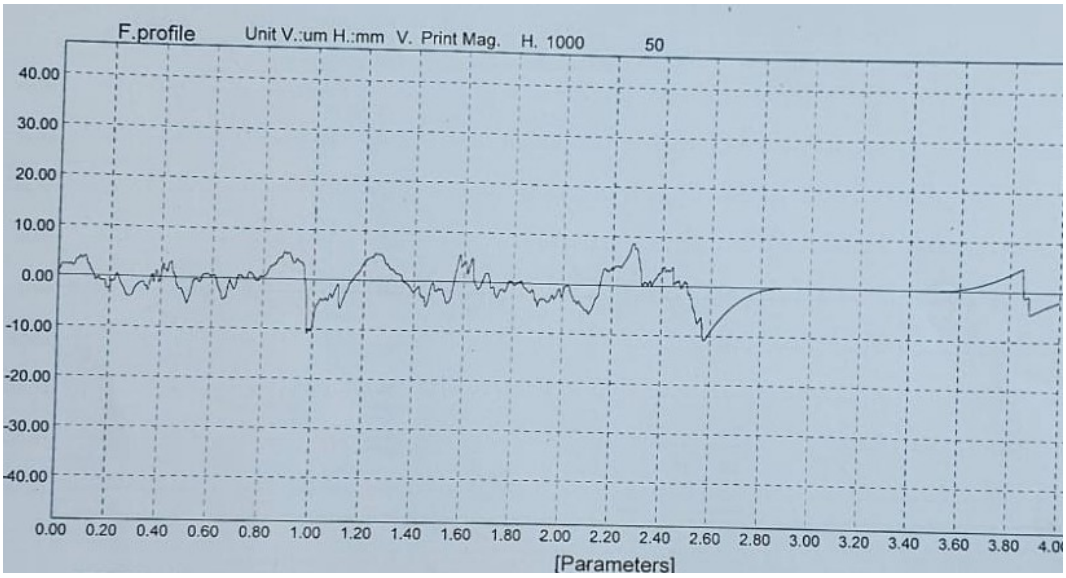

Figure 14 Assessment of surface roughness for the validation experiment

The values of experimentally determined kerf angle, entry and exit circularity, and the surface roughness were observed to be relatively close to the predicted values with only slight deviations that can be explained by intrinsic variations in the processes and measurement error as shown in Table 11. The high level of agreement is valid evidence that the developed models represent the necessary jet-material interaction behavior in the case of AWJM when drilling polycarbonate.

Table 11 Results of validation experiment

AWJM outcomes	Predicted value through SSO algorithm	Experimental value ((Mean ± SD)	% Error
Kerf angle-K_a (^{o})	0.597	0.582 ± 0.006	2.58
Entry circularity-C_{en} (mm)	0.717	0.689 ± 0.005	3.91
Entry circularity-C_{ex} (mm)	0.079	0.082 ± 0.002	3.80
Surface roughness S_r -(µm)	2.35	2.29 ± 0.04	2.21

The validation findings also indicate that the optimized parameter combination is effective in suppressing jet instability, reducing the amount of kerf deviation, and the amount of circularity retention with reasonable surface finish. These results reflect the usefulness of the suggested

ARTICLE IN PRESS

framework to the real-life context of AWJM operations, in which quality control and minimized trial-and-error learning are essential. The effective experimental confirmation supports the appropriateness of machine learning-based optimization as a decision support tool to achieve accurate polymer machining.

Conclusion

- This research developed a combined experimental and data-based platform of abrasive waterjet drilling of polycarbonate. The adequacy of the models was statistically proven, and quadratic models have described more than 92-94% of the total variability of the kerf angle, entry, and exit circularity, and surface roughness. The most influential factor on penetration-related responses was determined to be water pressure which contributed over 50% of the variation in kerf angle and exit circularity with standoff distance being the controlling factor of surface roughness with a contribution over 60% due to jet divergence effects. Coupled traverse rate-standoff interactions were the strongest predictors of entry circularity with more than 40% of its variation explained.
- As demonstrated by the machine learning models, Random Forest was able to achieve the greatest predictive accuracy on average geometric responses with R^2 values exceeding 0.82-0.94 and a 50 to 70% reduction in prediction errors relative to linear regression. The XGBoost best predicted surface roughness, indicating an R^2 of 0.93. The evolutionary optimization selected Salp Swarm Optimization as the best algorithm which provided the best drilling conditions of 250 MPa water pressure, 1.5 mm standoff distance, 300 mm/min traverse rate which gave low kerf angle (0.597) and entry and exit circularity (0.717 and 0.079) and controlled surface roughness (2.35 µm). Close correlation between the predicted and measured responses was proved by experimental validation.
- As demonstrated by the given ML-optimization framework, manufacturers can now drill polycarbonate parts using AWJM with

ARTICLE IN PRESS

high precision with minimal trial and error, with much better dimensional performance, and with much better surface integrity under well-defined optimum process conditions.

Scope for future study

Future studies may extend the present framework by investigating a wider range of AWJM process parameters to improve model generalization beyond the current experimental domain. The approach can be validated on different material systems, thicknesses, and composite structures to assess its broader applicability. In addition, incorporating larger experimental datasets with repetition along with detailed microstructural and subsurface damage analyses would further enhance model robustness and systematic understanding.

Data availability

The datasets used and/or analyzed during the current study are included in the published article.

The custom Python code and complete dataset used in this study are publicly available at:

https://github.com/lawansisa/Polycarbonate

ARTICLE IN PRESS

Funding

This article was co-funded by the European Union under the REFRESH – Research Excellence for Region Sustainability and High-tech Industries project number CZ.10.03.01/00/22_003/0000048 via the Operational Programme Just Transition and has been done in connection with project Students Grant Competition SP2024/087 Specific Research of Sustainable Manufacturing Technologies “financed by the Ministry of Education, Youth and Sports and Faculty of Mechanical Engineering VŠB-TUO. The article has been done in connection with the project Students Grant Competition SP2024/087”, Specific Research of Sustainable Manufacturing Technologies “financed by the Ministry of Education, Youth and Sports and Faculty of Mechanical Engineering VŠB-TUO”.

ARTICLE IN PRESS

Nomenclature

AWJM-Abrasive Waterjet Machining

ABR-Adaptive Boosted Regression

XGB-Extreme Gradient Boosting

DT-Decision Tree

RF-Random Forest

MLRM- Multi-linear Regression Model

BBO-Biogeography-Based Optimization

PSO-Particle Swarm Optimization

SSO-Salp Swarm Optimization

TWO-Tug-of-War Optimization

W_p-Waterjet Pressure

S_d-Standoff Distance

T_r-Traverse Rate

K_a-Kerf Angle

C_{en}-Hole Entry Circularity

C_{ex}-Hole Exit Circularity

S_r-Surface Roughness

CMM-Coordinate Measuring Machine

T-Thickness of the Material

ANOVA-Analysis of Variance

R^2–Coefficient of Determination

RMSE-Root Mean Square Error

MSE-Mean Square Error

MAE-Mean Absolute Error

RSE-Relative Standard Error

RAE-Relative Absolute Error

CC-Correlation Coefficient

CT-Computational Time

CIT-Convergence Iteration Number

CC-Convergence Value

OV-Multi-objective to Single objective

IGD-Inter Generated Distance

ARTICLE IN PRESS

ARTICLE IN PRESS

Div-Diversity
SP-Spacing
DV-Overall performance value based on Deng's method
EA-Evolutionary Algorithm

References

1. Zhang, W. and Xu, Y., 2019. Mechanical properties of polycarbonate: experiment and modeling for aeronautical and aerospace applications. Elsevier.
2. Getu, H., Ghobeity, A., Spelt, J.K. and Papini, M., 2008. Abrasive jet micromachining of acrylic and polycarbonate polymers at oblique angles of attack. Wear, 265(5-6), pp.888-901.
3. Madhu, S. and Balasubramanian, M., 2021. Challenges in abrasive jet machining of fiber-reinforced polymeric composites–a review. World Journal of Engineering, 18(2), pp.251-268.
4. Jahan, M.P., Ma, J., Hanson, C., Chen, X. and Arbuckle, G.K., 2020. Experimental and numerical investigation of cutting forces in micro-milling of polycarbonate glass. Machining Science and Technology, 24(3), pp.366-397.
5. Adeniji, D., Schoop, J., Gunawardena, S., Hanson, C. and Jahan, M., 2020. Characterization and modeling of surface roughness and burr formation in slot milling of polycarbonate. Journal of Manufacturing and Materials Processing, 4(2), p.59.
6. Jahan, M.P., Ma, J., Hanson, C. and Arbuckle, G.K., 2020. Tool wear and resulting surface finish during micro slot milling of polycarbonates using uncoated and coated carbide tools. Proceedings of the Institution of Mechanical Engineers, Part B: Journal of Engineering Manufacture, 234(1-2), pp.52-65.
7. Singh, K.J., Ahuja, I.S. and Kapoor, J., 2017. Mathematical modeling for material removal and optimization of ultrasonic drilling of polycarbonate and acrylic glass for surface roughness by GRA approach. International Journal of Mechanical Engineering and Applications, 5(3), pp.136-154.

ARTICLE IN PRESS

8. Vishwakarma, R. and Verma, R.K., 2021. Micro electric discharge machining (μ-EDM) of polymer nanocomposites modified by graphene nanoplatelets/carbon using rotating electrode tool. Journal of Micromechanics and Microengineering, 31(8), p.085010.
9. Moradi, M., Moghadam, M.K., Shamsborhan, M., Beiranvand, Z.M., Rasouli, A., Vahdati, M., Bakhtiari, A. and Bodaghi, M., 2021. Simulation, statistical modeling, and optimization of CO2 laser cutting process of polycarbonate sheets. Optik, 225, p.164932.
10. Moradi, M., Mehrabi, O., Azdast, T. and Benyounis, K.Y., 2017. Enhancement of low power CO2 laser cutting process for injection molded polycarbonate. Optics & Laser Technology, 96, pp.208-218.
11. Mishra, V., Sharma, R., Mahajan, K., Kumar, J., Khatri, N., Gupta, A., Garg, H., Karar, V., Pawade, R. and Sarepaka, R.V., 2021. Experimental investigations on ultra-precision machining of polycarbonate and related issues. Journal of Micromanufacturing, 4(1), pp.61-73.
12. Abdulwahab, A.E., Hubeatir, K.A. and Imhan, K.I., Optimization of Micro Drilling of Polycarbonate Using A Continuous CO2 Laser: An Experimental and Theoretical Comparative Study.
13. Singh, K.J., 2022. Chemical-assisted ultrasonic drilling of Polycarbonate bullet proof UL-752 glass and optimisation of process parameter by Taguchi, GRA and RSM approach. Advances in Materials and Processing Technologies, 8(1), pp.322-343.
14. Meena, R., Hashmi, A.W., Iqbal, F., Ahmad, S., Prakash, C., Katiyar, J.K., Mali, H.S. and Meena, A., 2024. Optimizing surface finish in FDM-printed polycarbonate spur gears through abrasive flow finishing: insights from physics and material science perspectives. Physica Scripta, 99(8), p.085004.
15. Faroze, F., Srivastava, V. and Batish, A., 2024. Modelling and prediction of mechanical properties of FFF-printed polycarbonate parts using ML and DA hybrid approach. Colloid and Polymer Science, 302(12), pp.1891-1909.
16. Zahmatkesh, S., Amiri, M.K., Zaferani, S.P.G., Emami, M.R.S., Hajiaghaei-Keshteli, M., Albaqami, M.D., Tighezza, A.M., Shafahi, M.

ARTICLE IN PRESS

and Han, N., 2023. Machine learning modeling of polycarbonate ultrafiltration membranes at different temperatures, Al2O3 nanoparticle volumes, and water ratios. Chemosphere, 313, p.137424.

17. Xiao, X.X., Bai, T.Y., Zhang, Q., Chen, Z.X., Wang, Z.N., Bai, J.H., Chen, L., Liu, B.W. and Wang, Y.Z., 2024. Machine learning-assisted design and scalable fabrication of high-performance fire-safe polycarbonate for advanced applications. Chemical Engineering Journal, 484, p.149565.
18. DeRudder, J.L., 1999. Commercial applications of Polycarbonates. In Handbook of Polycarbonate Science and Technology (pp. 319-332). CRC Press.
19. Elsner, J.J. and McKeon, B.P., 2017. Orthopedic application of polycarbonate urethanes: a review. Techniques in Orthopaedics, 32(3), pp.132-140.
20. Zhang, W. and Xu, Y., 2019. Mechanical properties of polycarbonate: experiment and modeling for aeronautical and aerospace applications. Elsevier.
21. Dahiya, A.K., Bhuyan, B.K., Acharya, V. and Kumar, S., 2023. Optimization of process parameters for machining defects of glass fibre reinforced polymer composite machined by AWJM. Materials Today: Proceedings.
22. Anand, G., Perumal, S.V., Yuvaraj, N. and Palanikumar, K., 2021. Influence of abrasive water jet machining parameters on hybrid polymer composite. Journal of The Institution of Engineers (India): Series C, 102(3), pp.713-722.
23. Arun, A., Rajkumar, K. and Vishal, K., 2023. Process parameters for optimization in abrasive water jet machining (AWJM) of silicon-filled epoxy glass fibre polymer composites. Journal of Inorganic and Organometallic Polymers and Materials, 33(5), pp.1339-1356.
24. Nagarajan, L., Mahalingam, S.K. and Vasudevan, B., 2024. Abrasive waterjet drilling process enhancement using machine learning and evolutionary algorithms. Materials and Manufacturing Processes, 39(15), pp.2166-2182.

ARTICLE IN PRESS

ARTICLE IN PRESS

25. Kumar, M.S., Nagarajan, L. and Vasudevan, B., 2024. Machinability study on abrasive waterjet drilling of YSZ-coated inconel 718 superalloy: optimization and modelling by machine learning. Engineering Research Express, 6(2), p.025425.
26. Periyappillai, G., Subbarayan, S. and Sengottaiyan, S., 2025. Advanced ensemble machine learning prediction to enhance the accuracy of abrasive waterjet machining for biocomposites. Materials Chemistry and Physics, 333, p.130175.
27. Ma, H., Simon, D., Siarry, P., Yang, Z. and Fei, M., 2017. Biogeography-based optimization: a 10-year review. IEEE Transactions on Emerging Topics in Computational Intelligence, 1(5), pp.391-407.
28. Rajesh, P.J., Balambica, V. and Achudhan, M., 2024, October. Advanced machining performance through optimization of awjm parameters using metaheuristic techniques. In Journal of Physics: Conference Series (Vol. 2837, No. 1, p. 012097). IOP Publishing.
29. Tamilarasan, A. and Renugambal, A., 2023. An Integrated RSM-improved salp swarm algorithm for quality characteristics in AWJM of Ananas comosus-HIPS composites. International Journal of Lightweight Materials and Manufacture, 6(3), pp.297-310.
30. Cayero, R., Rocandio, V., Zubillaga, A., Refoyo, I., Calleja-González, J., Castañeda-Babarro, A. and Martínez de Aldama, I., 2021. Analysis of tug of war competition: A narrative complete review. International Journal of Environmental Research and Public Health, 19(1), p.3.

ARTICLE IN PRESS